Kinetic selection of morphology and growth velocity in electrochemical deposition

F. Oberholtzer, D. Barkey, and Q. Wu
Department of Chemical Engineering, University of New Hampshire, Durham, New Hampshire 03824
(Received 26 November 1997; revised manuscript received 5 March 1998)

Ramified copper deposits were formed by electrochemical deposition from well supported acid sulfate solution under conditions of mixed kinetic and transport control. The growth velocity, morphology, and global rate of growth were measured over a range of applied driving force. Chloride was added to the solutions to modify the interfacial kinetics, and the kinetic parameters were obtained as a function of surface orientation by polarization measurements on copper single crystals. Chloride produces an anisotropic differential resistance to growth at the interface and a tendency toward high-velocity dendritic growth with formation of open low-density deposits. [S1063-651X(98)13406-2]

PACS number(s): 05.70.Ln, 68.70.+w, 81.15.Pq, 81.10.Dn

INTRODUCTION

In well supported electrolyte solutions, which present relatively little Ohmic resistance, ramified patterns can be produced by electrochemical deposition at low applied field strengths. As a result, the kinetic resistance at the interface accounts for a substantial portion of the total cell impedance and is experimentally accessible. Previously, we reported electrochemical growth of dendritic and tip-splitting deposits in solutions of cupric salts supported by sulfuric acid and compared these with indirect measures of the degree of anisotropy in the interfacial kinetic resistance [1]. It was shown that selection of fast growing dendritic morphologies is favored by addition of chloride to the solution, which increases the degree of anisotropy in surface kinetics. Here we present a more detailed characterization of the morphology and growth speed as well as direct measurement of the orientation-dependent kinetic resistance on copper single-crystal surfaces.

Electrochemical deposition differs from precipitation or solidification in that the crystallization process is accompanied by chemical transformations. The chemical nature of the process has recently been investigated for ramified deposition in thin layers, and it has been shown that the chemical environment may affect the morphology by modifying the surface processes [1–8] or the transport properties of the solution near the interface [9–11].

The three species of copper present in our deposition experiments are the metal Cu, the cupric ion Cu^{2+} and the cuprous ion Cu^{1+}. They are coupled by two elementary electrochemical reactions at the interface.

$$Cu^{2+} + e^- \Leftrightarrow Cu^{1+}, \tag{1}$$

$$Cu^{1+} + e^- \Leftrightarrow Cu. \tag{2}$$

Deposition is produced when reactions (1) and (2) are forced from left to right, so that the overall reaction is

$$Cu^{2+} + 2e^- \Rightarrow Cu. \tag{3}$$

If reaction (3) proceeds with 100% current efficiency, and atoms are incorporated into the solid near the point of discharge, the growth velocity v and current density i at a point on the surface are related by

$$v = \left(\frac{\hat{V}}{nF} \right) i, \tag{4}$$

where $\hat{V}$ is the molar volume of the metal and nF the number of coulombs passed per mol of metal deposited. If, on the other hand, the surface-diffusion length for adatoms is not small in comparison with the features of the deposit, the local rate of growth is not necessarily proportional to the local current density. We will assume that Eq. (4) holds under the conditions of our experiments.

The current density is a function of the applied driving force or overpotential η, which may be decomposed into three additive components. These are the Ohmic overpotential η_Ω, the concentration overpotential η_c, and the surface overpotential η_s:

$$\eta = \eta_\Omega + \eta_c + \eta_s. \tag{5}$$

The total overpotential η is imposed through the external circuit and has the same value over any path from the reference electrode to the deposit. The component overpotentials, on the other hand, depend on the path, and the distribution of current density is a function of the distribution of resistances offered by the solution and the surface. Procedures for determining current densities around stationary or slowly advancing electrodeposits have been worked out for many electrochemical deposition systems. The Ohmic and concentration overpotentials depend only on solution properties, deposit geometry, and current density. However, the surface overpotential depends as well on the properties of the interface, including the metal surface and the double layer.

The relation between η_s and i can be expressed by the differential surface resistance, defined as

$$r_s = \frac{\partial \eta_s}{\partial i}. \tag{6}$$

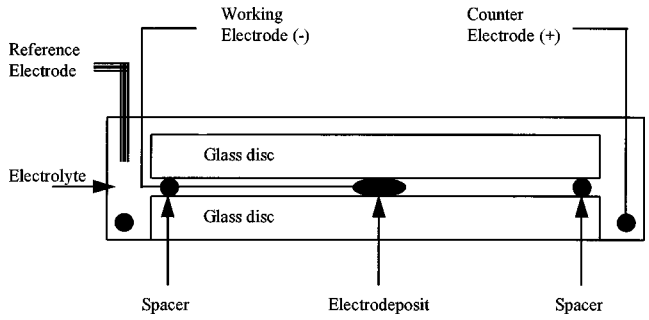

FIG. 1. Thin-layer electrochemical cell with reference electrode and anode compartment.

The objective of our experiments was to relate r_s to the morphology. The discharge of an ion and its incorporation into the solid phase proceeds through a series of steps that include dehydration, electron transfer, surface diffusion, and attachment. Each of these can be influenced by the surface structure and the presence of adsorbed anions or salt films, and the detailed mechanism is not accessible to the present experiments. However, the surface resistance, which is measurable, represents a sum of resistances offered by the individual steps, and it captures the overall effect of interfacial processes on the macroscopic distribution of current and surface growth.

EXPERIMENTAL METHODS

Copper electrodeposits were formed in the thin-layer cell shown in Fig. 1. The cell consisted of two circular glass plates 8 cm in diameter stacked in a 10 cm glass petri dish. The plates were separated by ten strips of PTFE 100 μm thick, 1 mm wide and 10 mm long laid near the edge of the plates and oriented in the radial direction. PTFE seating rings were placed above and below the glass plates and pressed into position with dogging devices to ensure that the space between the plates was level and uniform in thickness. The filled cell contained 15 to 20 cm^3 of solution, with roughly 0.5 cm^3 between the plates where the deposit was formed. The composition of the electrolyte solution was 0.5*M* $CuSO_4$–0.5*M* H_2SO_4 (sulfate solution) or 0.5*M* $CuSO_4$–0.5*M* H_2SO_4–0.0022*M* KCl (chloride solution). Solutions were prepared with reagent grade chemicals and water purified with a Nanopure II ultrafiltation system.

Deposits were grown from the exposed end of a copper wire, 50 μm in diameter, with a 2 μm insulating coating of polyesterimide. The counter electrode was a circular piece of bare copper wire placed in the petri dish outside of the plates. The deposits were formed at a constant potential with respect to a mercury–mercurous sulfate reference electrode connected to the cell through a bridge tube filled with 1.0*M* sulfuric acid. The aggregate radius was measured with sequential photographs of the deposit.

Kinetic measurements were carried out with copper single-crystal electrodes in a three electrode cell in the same solutions used in the deposition experiments. The cell consisted of a 50 ml glass vessel, with counterelectrode and reference-electrode compartments separated from the main compartment by porous frits. The counterelectrode, which collects the current imposed on the working electrode, was a carbon rod. The reference electrode was a mercury-mercurous sulfate electrode. The working electrodes were single-crystal copper disks, 12 mm in diameter, with orientations of (100), (110), (111), and (321). These were polished mechanically with 0.05 μm alumina and electropolished in orthophosphoric acid. They were mounted in the hanging mensicus arrangement to confine contact with the solution to the polished face. The Ohmic resistance of the cell was determined by measurement of the high-frequency (100 kHz) impedance. The overpotential as a function of applied current was then determined by application of a controlled current for 10 ms. The concentration overpotential was assumed to be zero because the current pulse was short compared to the time required to deplete the solution at the interface. The Ohmic overpotential was calculated by multiplying the applied current by the measured cell resistance. The surface overpotential was then found by subtracting η_Ω from the measured total overpotential.

RESULTS

Typical plots of aggregate radius versus time for sulfate solution and for chloride solution are shown in Figs. 2(a) and 2(b), respectively. To compare velocities at different potentials, we took the slope of the radius versus time curves at two points. One velocity was taken at an aggregate radius of 0.16 mm and a second was taken at an aggregate radius of 1.0 mm or after 4 h, whichever came first. These velocities are plotted against overpotential in Fig. 3, where the open symbols are the first velocity and the filled symbols are the second. In all cases, the velocity decreased by a factor of about two between these limits.

The velocities in chloride solution are about ten times larger than the velocities in sulfate solution over most of the range of applied overpotential. In sulfate solution, there is a jump in velocity at an overpotential of 600 mV, while in chloride solution, there is a drop in velocity at the same point. These shifts correspond to changes in morphology as discussed below.

Figure 4 shows deposits formed in sulfate solution at several overpotentials. At the lowest driving force, the emergence of branches was slow, and the deposit was nearly circular early in the experiment. At higher overpotentials, branching occurred earlier, the radius of the branch tips was smaller, and the tips split more frequently. At an overpotential of 600 mV, the highest driving force accessible before the onset of hydrogen evolution, the branches were dendritic, and grew much faster than those formed at 550 mV.

In chloride solution, dendrites were produced over most of the range of applied overpotential (see Fig. 5). At driving forces between 250 and 400 mV, the branches were dendritic but frequently emitted new branches with different growth directions. At 450 and 500 mV, the morphology was dendritic, with stable central needles, regular side branches, and tertiary branching. At 550 mV, the branches again emitted new branches frequently, and at 600 mV, the deposit was dark, its shape was dominated by tip splitting, and no central needle crystals were visible. The deposits formed at 600 mV grew at a lower velocity than those formed at 550 mV.

Figure 6(a) shows the cell current plotted against time for deposits formed in sulfate solution at overpotentials of 400

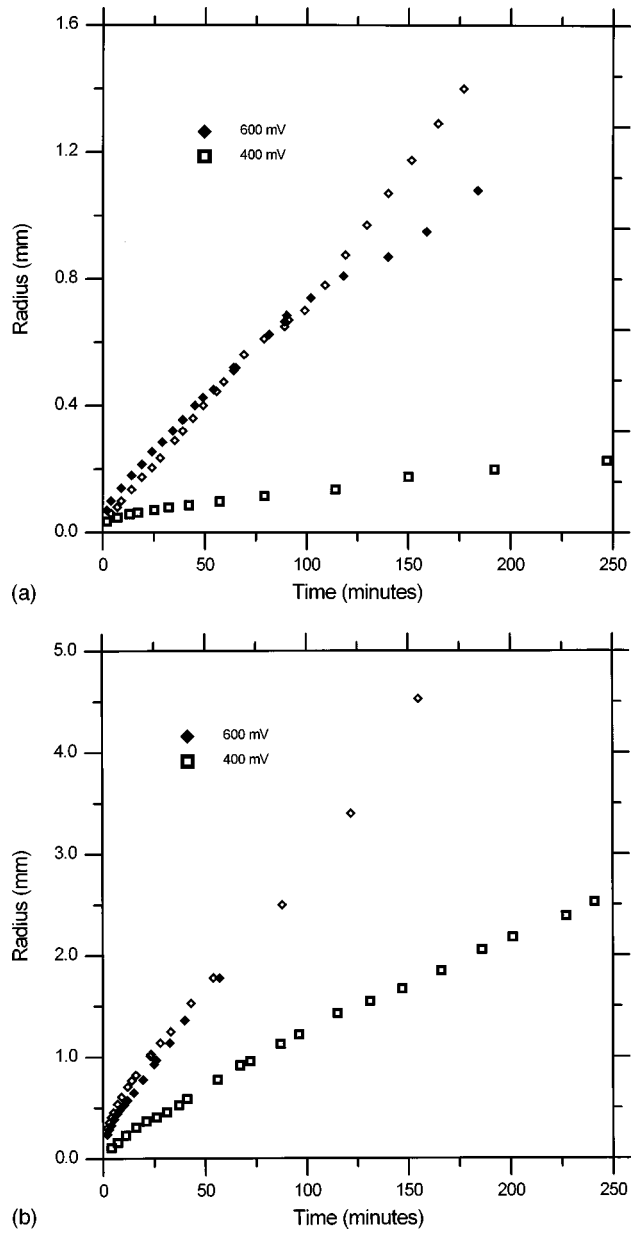

FIG. 2. Radius vs time. (a) Deposits formed in sulfate solution at overpotentials of 400 and 600 mV. (b) Deposits formed in chloride solution at overpotentials of 400 mV and 600 mV.

and 600 mV. The current increases very rapidly at first as the surface area of the deposit increases and the Ohmic resistance decreases steeply. However, deposition depletes the interfacial concentration of the metal ion, and the current eventually rises at a slower steady rate. The corresponding plot for the chloride solution is shown in Fig. 6(b). Here, the dendritic deposit grown at 400 mV follows the same pattern as in the sulfate solution. However, at 600 mV, where the deposit grows by tip splitting, the current reaches a maximum and then declines. As discussed below, this drop in current is evidence that a film of cuprous chloride has precipitated on the metal.

The cell current, sampled in each experiment at a deposit radius of 0.16 mm, is plotted against overpotential in Fig. 7. The current is greater in chloride solution than in sulfate solution, but the contrast in current is much smaller than the contrast in growth velocity. As a result, the deposits formed

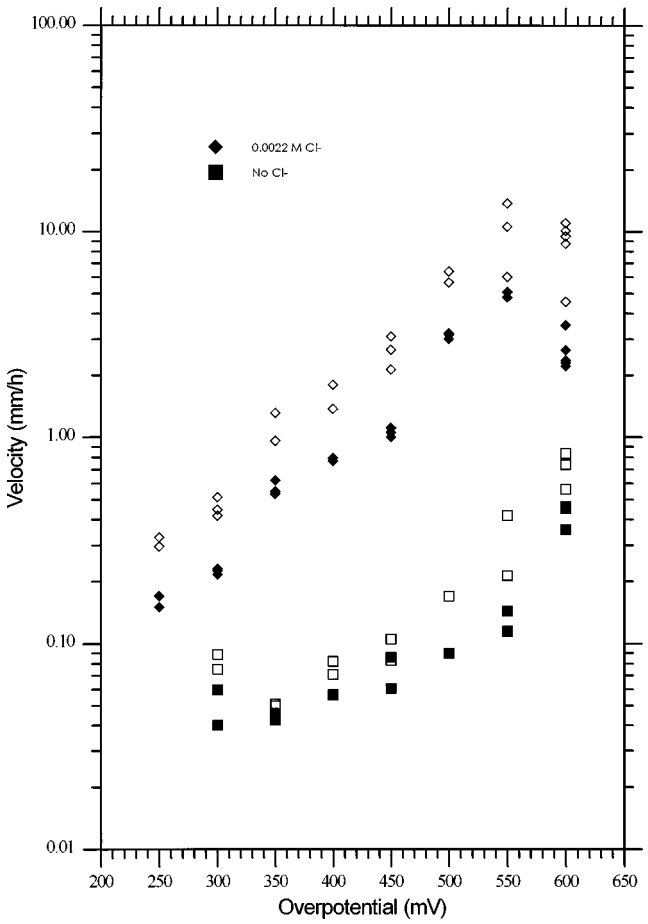

FIG. 3. Velocity v vs overpotential η for sulfate and chloride solution. The open symbols represent velocities measured at a radius of 0.16 mm, and the filled symbols velocities measured at 1.0 mm or 240 min.

in chloride solution are more open and less dense than those formed in sulfate solution. This can be seen by comparison of the time integral of current, or total charge passed, at a deposit radius of 0.16 mm (Fig. 8). A solid deposit at this radius is equivalent to 220 mCoulombs, while the densest deposit obtained, formed at 300 mV in sulfate solution, was equivalent to 150 mCoulombs and the least dense, formed at 550 mV in chloride solution, to 0.8 mCoulombs. The void fraction thus ranged from 32% to more than 99%.

A condition of zero current does not assure equilibrium, and in solutions exposed to air, equilibrium is generally impossible to obtain. Moreover, our solutions were made up with cupric salts, and in chloride solution the cuprous ion is stabilized by formation of chloride complexes. We therefore computed the solution composition that would result from excluding oxygen from the electrolysis cell and allowing the solution and metal to come to equilibrium. This process would occur by reaction of cupric ion with the metal to form the curprous ion and by formation of chloride complexes in solution. Stability constants for the complexes are shown in Table I [12,13]. Table II shows the composition of the chloride solution at equilibrium. The liquid-phase composition is not very different from that of the sulfate solution, and nearly all of the copper in solution is the uncomplexed Cu^{2+}. However, the specie CuCl is saturated and a solid phase of this compound is present at equilibrium. This fact alone does not

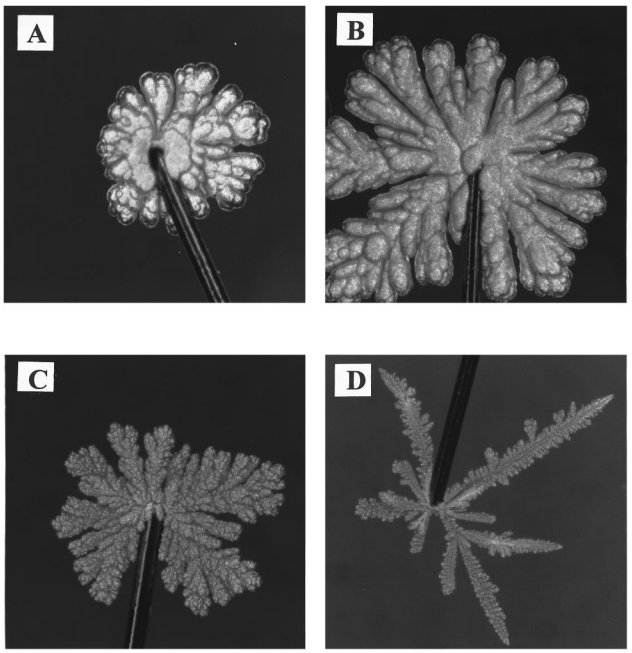

FIG. 4. Deposits formed in sulfate solution at overpotentials of (a) 300 mV, (b) 400 mV, (c) 500 mV, (d) 600 mV. The width of the wire is 50 μm, and the field of view is 1.25 mm.

assure that CuCl will precipitate in the experiments because these occur under nonequilibrium conditions.

The kinetic parameters were found by plotting $\log(i)$ against η_s for the single-crystal disk electrodes. In sulfate solution (Fig. 9) the rate of deposition is controlled by discharge of Cu^{2+} to Cu^{1+}, as shown by the slope of the polarization curves in the limit of high overpotential ($\eta_s > 70$ mV). In this region they can be represented by [14,15]

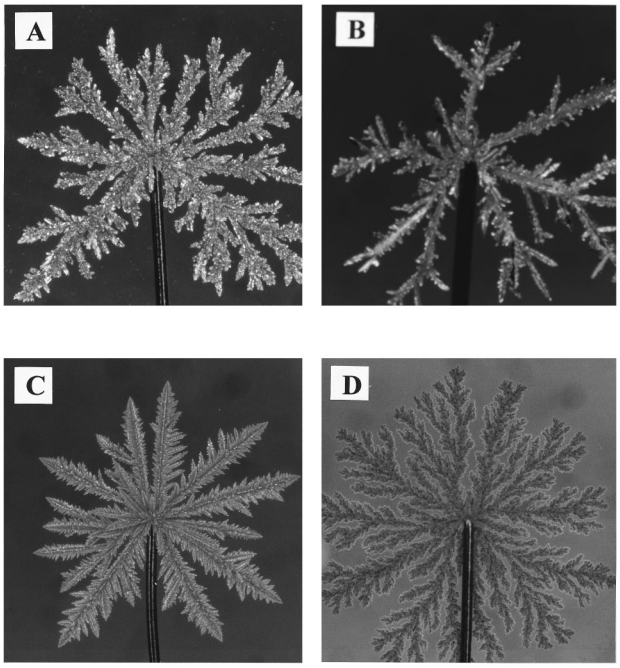

FIG. 5. Deposits formed in chloride solution at overpotentials of (a) 300 mV, (b) 400 mV, (c) 500 mV, (d) 600 mV. The width of the wire is 50 μm, and the field of view is 1.25 mm.

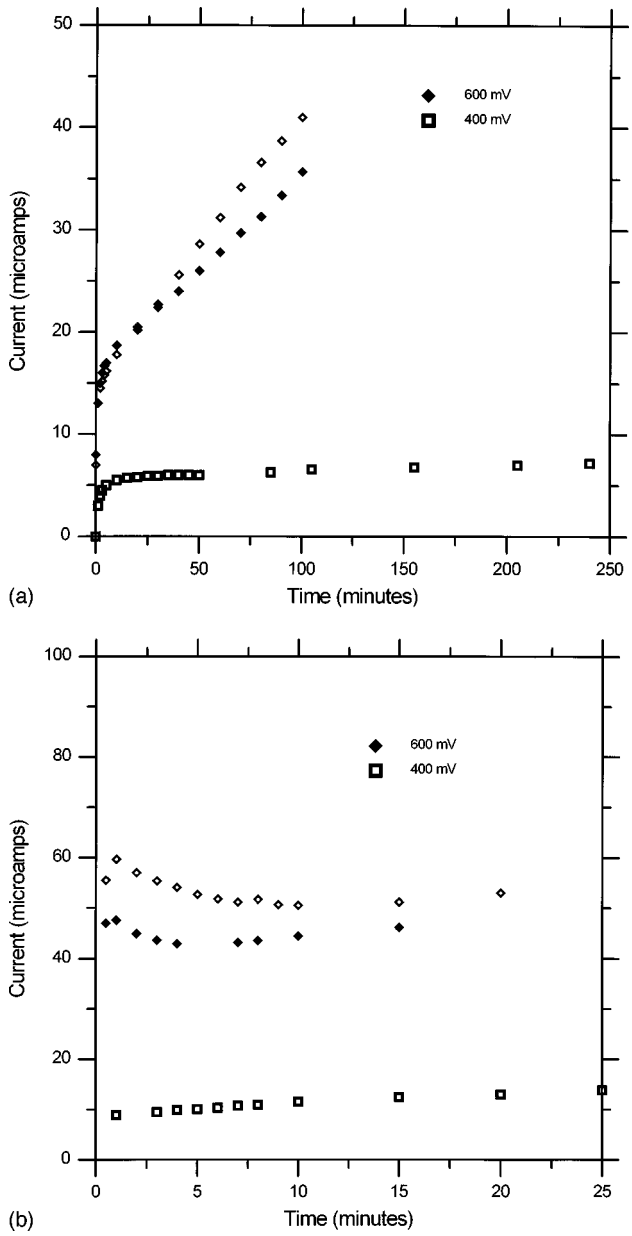

FIG. 6. Cell current I vs time. (a) Sulfate solution for a tip-splitting deposit (400 mV) and a dendritic deposit (600 mV). (b) Chloride solution for a dendritic deposit (400 mV) and a tip-splitting deposit (600 mV).

$$\log(i) = \log(i_0) + \frac{\eta_s \alpha n F}{2.3RT}, \tag{7}$$

where α and i_0 are kinetic constants. α is equal to 0.5 for all three surfaces, and i_0 contains all of the anisotropy in the kinetics. Consistent with previous measurements, i_0 decreases in the order (110)>(100)>(111) [16]. In dilute chloride solution (Fig. 10), the kinetic behavior is not described by Eq. (8) and so deposition from chloride solution is not entirely a discharge controlled mechanism. An additional impedance is presented by the crystallization process.

DISCUSSION

Over most of the available range of driving force, deposition in chloride solution produces dendrites while deposi-

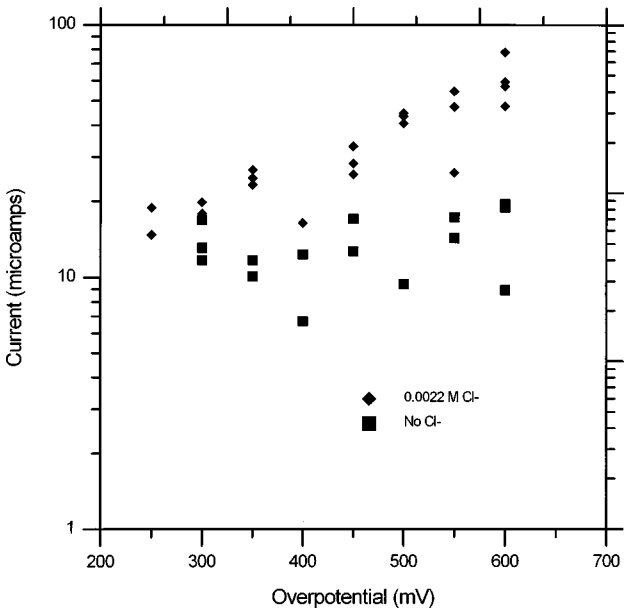

FIG. 7. Cell current I vs overpotential η.

tion in sulfate solution produces tip splitting. The exception is near the maximum driving force before the onset of hydrogen evolution, where dendrites grow in sulfate solution and deposits in chloride solution turn dark and tip split.

While chloride has little effect on the transport properties of the solutions, its effect on the interfacial resistance is substantial, as can be seen in Fig. 10. The polarization curves for sulfate solution indicate a process controlled by discharge of the divalent ion by reaction (1) [14,15]. They follow the form of Eq. (8), and the differential resistance r_s is uniform among the faces. In contrast, the differential resistance in chloride solution is strongly anisotropic. The polarization curve for the (100) surface deviates markedly from the other curves, and r_s is not uniform in the high current region. Evidently, deposition in this solution is not controlled by discharge alone, but is strongly influenced by surface-specific factors, probably including a monolayer of adsorbed chloride [17].

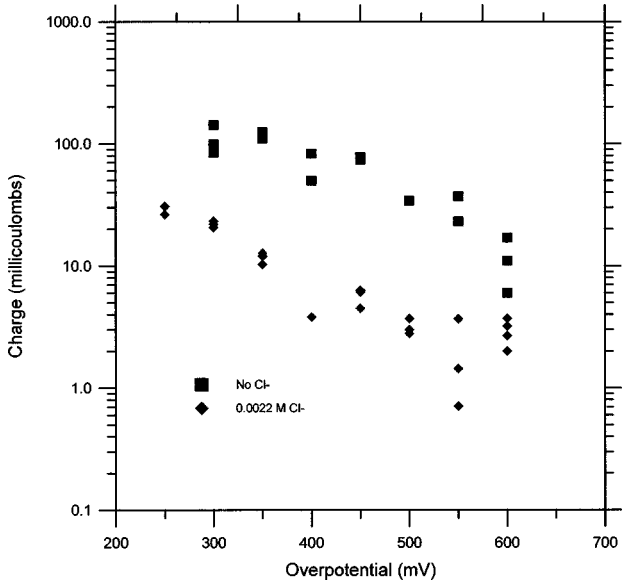

FIG. 8. Equivalents deposited at a radius of 0.16 mm vs overpotential η.

TABLE I. Stability constants for chloride complexes of copper in aqueous solution.

Species	Stability constant
CuCl	5.01×10^{2}
$CuCl_2^-$	1.15×10^{6}
$CuCl_3^{2-}$	1.00×10^{6}
$Cu_2Cl_4^{2-}$	1.00×10^{13}
$CuCl^+$	2.31
$CuCl_2$	0.65
$CuCl_3^-$	0.38

The differential resistance r_s is the term that represents surface kinetics in stability analyses of electrodeposition because it governs the response of local current densities to variations in overpotential on perturbations [18]. Presumably it is this term that determines the response to small fluctuations near a growth tip as well. In sulfate solution, r_s is the same for all orientations, and tip splitting is produced at most driving forces. In chloride solution, r_s depends on orientation, and dendrites are produced at most driving forces. This result is consistent with the view that interfacial anisotropy is required to stabilize dendritic growth [19].

The tip splitting growth produced at very high growth rate in the chloride solutions is accompanied by a color change, evidence that a precipitate has formed on the metal. Similar transitions are well documented in binary solution and have been attributed to pH shifts [20–23]. In the present experiments, the pH is much lower than in binary copper sulfate, and copper oxides are not likely to precipitate. Moreover, in these well supported solutions, the pH does not vary appreciably in the vicinity of the deposit. Precipitation of copper oxides is therefore not likely to cause the color change in our experiments. On the other hand, our calculation of the equilibrium compositions shows that cuprous chloride is present in supersaturation, and a film of cuprous chloride may form on the metal. If transport across the film were rate limiting, the anisotropy in kinetics shown in Fig. 10 would no longer control the selection of morphology at the tip.

TABLE II. Molar concentrations of chloride complexes of copper at equilibrium. The asterisk indicates the molar quantity of CuCl, which would precipitate from one liter of solution made up with $0.5M$ of $CuSO_4$ and $0.0022M$ of KCl.

Species	Molar concentration
Cu^{2+}	4.99×10^{-1}
Cu^+	5.73×10^{-5}
$CuCl^+$	8.39×10^{-4}
$CuCl_{(s)}$	$5.41\times10^{-4}*$
$CuCl_{(aq)}$	2.09×10^{-5}
$CuCl_2^-$	3.49×10^{-5}
$CuCl_3^{2-}$	2.21×10^{-8}
$Cu_2Cl_4^{2-}$	9.22×10^{-9}
$CuCl_2$	3.97×10^{-7}
$CuCl_3^-$	1.10×10^{-10}

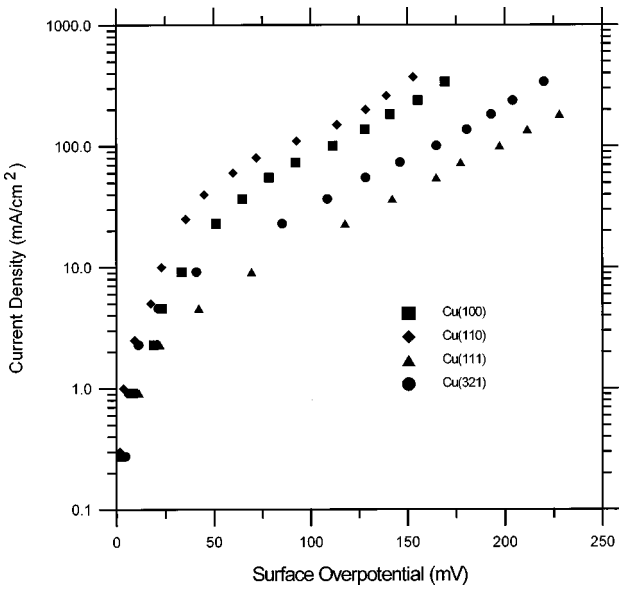

FIG. 9. Log of current density i vs surface overpotential η_s (Tafel plot) for copper single crystals in sulfate solution, $0.5M$ $CuSO_4/0.5M$ H_2SO_4.

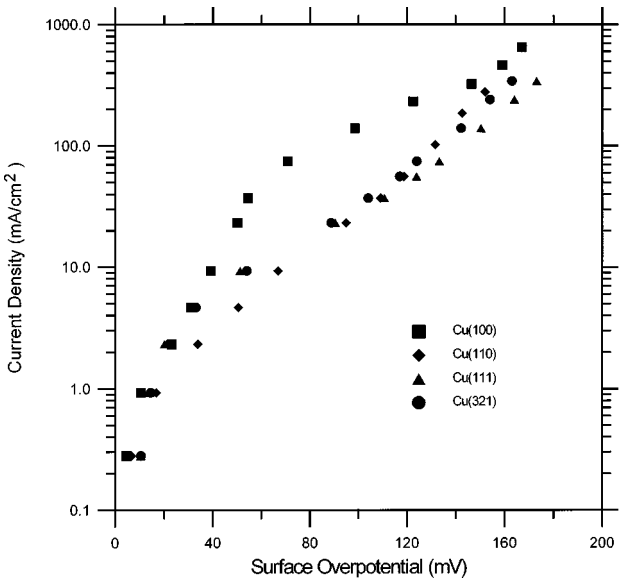

FIG. 10. Log of current density i vs surface overpotential η_s (Tafel plot) for copper single crystals in chloride solution, $0.5M$ $CuSo_4/0.5M$ $H_2SO_4/0.0022M$ KCl.

The appearance of dendrites in sulfate solution at 600 mV cannot be accounted for with our kinetic data. Kinetic measurements on planar electrodes may not reflect the real limiting steps for high-speed growth at sharply curved tips. One possibility is that the morphology is dominated at very high overpotential by twinning processes, which are not captured in the kinetic data shown in Fig. 9 [24,25].

The contrast in velocity between solutions is much larger than the contrast in material flux to the deposits because the current density in dendritic growth is concentrated onto fast-growing tips of small radius. There is some difference in current density, however, and so we examine the transport mechanisms likely to dominate mass transfer in this system. We assume that all of the current passing into the solid does so by discharge of cupric ion (100% current efficiency). The migration flux of cupric ion is given by the fraction of the current that is carried by movement of cupric ion in solution. For our solutions, this fraction is roughly 0.1 so that migration accounts for a small part of the material flux.

An additional source of material at the interface is provided by advection, or the relative motion of the growth front and the solution. The maximum current i_a that can be supported by advection alone is given by [26–28]

$$i_a = nFC_b v, \tag{8}$$

where C_b is the concentration of metal ion in the bulk of the solution. The highest velocity we measured was roughly 10 mm/h, which gives a maximum advection current of about 30 μA at a deposit radius of 0.16 mm, or one-tenth of the observed current. At lower velocities, the advection term decreases more rapidly than the measured currents. We conclude that migration and advection together account for no more than 20% of the material flux.

The most important transport mechanism in these experiments is convective diffusion. The maximum convective diffusion flux can be estimated from dimensionless correlations as follows. The convective-diffusion limited current density is given by

$$i_L = \frac{nFDC_b}{L}\,\mathrm{Sh}, \tag{9}$$

where Sh is the Sherwood number, D the diffusivity of the metal ion, and L the plate spacing. For natural convection [29,30],

$$\mathrm{Sh} = (\mathrm{Gr}\,\mathrm{Sc})^{0.25}, \tag{10}$$

where the Grashof and Schmidt numbers are defined by

$$\mathrm{Gr} = \frac{g\Delta\rho L^3}{\rho_{\mathrm{inf}}\nu^2},$$

$$\mathrm{Sc} = \frac{\nu}{D}.$$

ρ is the solution density, $\Delta\rho$ the density difference between the bulk and the fully depleted solution, and ν the kinematic viscosity. The solution parameters were estimated with correlations [31], and the diffusivities were taken from previous measurements [32]. The maximum convective-diffusion flux for the present experiments is roughly 200 μA at a deposit radius of 0.16 mm. This figure is larger than the maximum recorded current ($\approx$100 μA). We conclude that natural convection accounts for most of the material flux in our system, and growth of the aggregates always takes place well below the transport-limited current. This is consistent with the view that the rate of growth is limited by interfacial kinetics as well as material transport.

CONCLUSION

The morphology and growth velocity of ramified deposits formed by electrochemical deposition of copper are controlled in part by interfacial kinetics. The global rate of growth is significantly lower than the transport limited rate, and modification of the activated processes at the interface can produce large changes in the overall process. Over most of the accessible range of driving force, there is a correspondence between kinetic parameters obtained on single crystals and the morphology observed in ramified deposition. In sulfate solution, the kinetics are controlled by ionic discharge in solution, an isotropic process that results in tip-splitting growth. In the presence of chloride, surface processes become important, the differential resistance to growth is anisotropic, and dendrites or faceted fingers are formed. The transition from tip splitting to dendrite growth is accompanied by large increases in growth velocity and void fraction.

ACKNOWLEDGMENTS

This work was supported by the National Science Foundation under Grant Nos. CTS-9306837 and CTS-9622634, and by the NATO Scientific Affairs Division under Grant No. CRG-930546. The authors thank Peter Garik, Fransesc Sagues, and Josep Claret for many helpful discussions.

[1] D. Barkey, F. Oberholtzer, and Q. Wu, Phys. Rev. Lett. **75**, 2980 (1995).
[2] A. Kuhn and F. Argoul, Phys. Rev. E **49**, 4298 (1994).
[3] V. Fleury, M. Rosso, J. N. Chazalviel, and B. Sapoval, Phys. Rev. A **44**, 6693 (1991).
[4] A. Kuhn and F. Argoul, J. Electroanal. Chem. **371**, 93 (1994).
[5] A. Kuhn and F. Argoul, Phys. Rev. Lett. **73**, 2998 (1994).
[6] F. Argoul and A. Kuhn, J. Electroanal. Chem. **359**, 81 (1993).
[7] F. Argoul and A. Kuhn, Physica A **213**, 209 (1995).
[8] M. Wang and N. Ming, Phys. Rev. Lett. **71**, 113 (1993).
[9] P. P. Trigueros, J. Claret, and F. Sagues, Phys. Rev. E **49**, 4328 (1994).
[10] M. Q. Lopez-Salvans, P. P. Trigueros, S. Vallmitjana, J. Claret, and F. Sagues, Phys. Rev. Lett. **76**, 4062 (1996).
[11] M. Q. Lopez-Salvans, F. Sagues, J. Claret, and J. Bassal, J. Electroanal. Chem. **421**, 205 (1997).
[12] R. M. Smith and A. E. Martell, *Critical Stability Constants, Inorganic Complexes* (Plenum, New York, 1976), Vol. 4; *Critical Stability Constants, First Supplement* (Plenum, New York, 1982), Vol. 5.
[13] R. W. Ramette and G. Fan, Inorg. Chem. **22**, 3323 (1983); R. W. Ramette, *ibid.* **25**, 2481 (1986).
[14] E. Mattson and J. O'M. Bockris, Trans. Faraday Soc. **55**, 1586 (1959).
[15] O. R. Brown and H. R. Thirsk, Electrochim. Acta **10**, 383 (1965).
[16] A. Damjanovic, T. H. V. Setty, and J. O'M. Bockris, J. Electrochem. Soc. **113**, 429 (1966).
[17] I. Villegas, C. B. Ehlers, and J. L. Stickney, J. Electrochem. Soc. **137**, 3143 (1990).
[18] D. Barkey, R. H. Muller, and C. W. Tobias, J. Electrochem. Soc. **136**, 2207 (1989).
[19] E. Ben-Jacob and P. Garik, Nature (London) **343**, 523 (1990).
[20] D. Barkey, P. Garik, E. Ben-Jacob, B. Miller, and B. Orr, J. Electrochem. Soc. **139**, 1044 (1992).
[21] D. B. Hibbert and J. R. Melrose, Proc. R. Soc. London, Ser. A **423**, 149 (1989).
[22] J. R. Melrose, D. B. Hibbert, and R. C. Ball, Phys. Rev. Lett. **65**, 3009 (1990).
[23] V. Fluery, J. Chazalviel, M. Rosso, and B. Sapoval, J. Electroanal. Chem. **290**, 249 (1990).
[24] F. Ogburn, J. Electrochem. Soc. **111**, 870 (1964).
[25] V. Fleury and D. Barkey, Europhys. Lett. **36**, 253 (1990).
[26] D. P. Barkey and P. D. LaPorte, J. Electrochem. Soc. **137**, 1655 (1990).
[27] D. P. Barkey, J. Electrochem. Soc. **138**, 2912 (1991).
[28] D. P. Barkey, P. Garik, E. Ben-Jacob, B. Miller, and B. Orr, J. Electrochem. Soc. **139**, 1044 (1992).
[29] N. Ibl, Electrochim. Acta **1**, 117 (1959).
[30] C. Wagner, J. Electrochem. Soc. **124**, 129 (1957).
[31] S. K. Arapkoske and J. R. Selman, University of California-Berkeley, Lawrence Radiation Laboratory Report No. UCRL-20510, 1971.
[32] J. T. Hinatsu and F. R. Foulkes, J. Electrochem. Soc. **136**, 125 (1989).